Audio Engineering Society

Convention Paper 10046

Presented at the 145th Convention
2018 October 17 – 20, New York, NY, USA

Numerical Optimization Strategies for Acoustic Elements in Loudspeaker Design

Andri Bezzola[1]

[1]*Samsung Research America, DMS Audio, Valencia CA 91355*

Correspondence should be addressed to Andri Bezzola (andri.b@samsung.com)

ABSTRACT

Optimal design of acoustic loudspeaker design elements, such as waveguides and phase plugs, often requires extensive experience by the designer. Numerical simulations and optimization algorithms can aid in reducing the design-test-optimize cycle that is traditionally applied. A general mathematical framework for numerical optimization techniques is introduced and three algorithms of design optimization are reviewed: parameter optimization, shape optimization, and topology optimization. This paper highlights strengths and drawbacks of each method with the use of real-world design of a waveguide and two phase plugs. Where possible, the results are confirmed with prototypes and measurements. The work shows that excellent results can be achieved in just one design iteration with the help of numerical optimization methods.

1 Introduction

1.1 Background

Loudspeaker design has made tremendous progress using numerical simulations in the past several decades. The availability of easy-to-use software with graphical user interfaces and predefined physics setups has advanced the types of numerical simulations that loudspeaker designers employ to improve their products. Finite Element Models (FEM) have led to accurate models predicting acoustic diffraction and directivity of speaker cabinets and waveguides [1], acoustic impedance of horns [2], turbulence studies in port tubes [3], breakup modes of diaphragms [4], transducer linear and nonlinear behavior [5, 6, 7, 8], and many other applications [9].

The design process often requires the iteration of simulation and adaptation of the geometry. Such is certainly the case when optimizing acoustic elements because the measure of directivity is directly linked to the geometry. Sometimes a loudspeaker designer can refer to analytical solutions to determine the optimal design, but such solutions are not always available, particularly when the geometry at hand cannot be described by basic shapes such as spheres, boxes, cylinders etc. The designer then often needs to start with a best guess and iterate through several loops of simulation and geometry adaptation until a satisfactory solution is found. Thanks to modern simulation software and capable hardware, this kind of "manual" optimization is still faster than building prototypes and measuring them.

Numerical optimization methods can aid the designer

by systematically finding geometries that are closer to the optimal design. It is the intention of this work to describe 3 optimization strategies that can be used in loudspeaker design. These three strategies are:

1. Parameter Optimization
2. Shape Optimization
3. Topology Optimization

The requirements, strengths and drawbacks of each methods are illustrated with practical examples. But first we need to define a general optimization problem statement.

1.2 General Optimization Problem Definition

The general aim of an optimization algorithm is to find the set of control variables that maximize or minimize a real scalar function. (For the sake of brevity, we will stick to minimization problems in this work, as any maximization problem can easily be transformed into a minimization problem by taking the inverse or negative of the optimization function.) To formalize this general description we need some definitions:

- Objective function $F(\mathbf{q})$: The objective function (also called target or cost function) is the measure that is to be optimized. It returns a scalar value
- Control variables $\mathbf{q}$: Control variables are the variables that the algorithm is iteratively varying in order to find the mimimum of the objective function. The set of variables that optimizes F is defined as $\bar{\mathbf{q}}$.
- Constraints $\mathbf{G}(\mathbf{q})$: The searchable space for the optimal control variables can be restricted by the vector-valued expression $\mathbf{G}$. A set of $\mathbf{q}$ that does not violate any constraints is called a feasible set $\mathbf{C}$.

In mathematical terms, the optimization problem is then defined as :

Find $\bar{\mathbf{q}}$ such that

$$\begin{cases} \bar{\mathbf{q}} = \min\limits_{\mathbf{q}} F(\mathbf{q}) \\ \mathbf{C} = \{\mathbf{q} : \mathbf{lb} \leq \mathbf{G}(\mathbf{q}) \leq \mathbf{ub}\} \end{cases} \tag{1}$$

where $\mathbf{lb}$ and $\mathbf{ub}$ are the vectors containing the lower and upper bounds of $\mathbf{G}(\mathbf{q})$.

This general description applies to all three optimization strategies mentioned above. Where they differ is in the choice of control variables $\mathbf{q}$ and how they are tied to the geometry definition. In the following sections, there will be a description of each method followed by a loudspeaker design example.

2 Parameter Optimization

Parametric Computer Aided Design (CAD) allows for the quick variation of geometries by keeping certain key dimensions as variables. Such key dimensions can be point coordinates, line lengths, radii, coefficients of polynomials, spline parameters, etc. For example, a simple conical diaphragm can be dimensioned parametrically by its diaphragm depth d, thickness t, inner radius R_i, and outer radius R_o, or - alternatively - by d, t, R_i, and flare angle α. It is up to the designer to determine how to best parameterize the geometry.
It is always advisable to map the parametrization with control variables that take on values between 0 and 1 (or sometimes between -1 and 1). For example, if the outer diameter of the diaphragm above can vary between R_o^{min} and R_o^{max}, then the linear mapping

$$R_o^{feas} = R_o^{min} + q_{R_o}\left(R_o^{max} - R_o^{min}\right); \quad q_{r_o} \in (0,1) \tag{2}$$

uses the control variable q_{R_o} to define all feasible outer radii. In the optimization of the above cone, we can then define the optimization control variables $\mathbf{q}$ as

$$\mathbf{q} = [q_d, q_t, q_{R_i}, q_{R_o},]^T \tag{3}$$

and the constraints become simply

$$0 \leq \mathbf{q} \leq 1. \tag{4}$$

This change of variables from design parameters to control parameters is not required, but the normalization can benefit stability and performance of the optimization algorithms [10].

During the optimization run, the algorithm continuously updates the control parameters in order to achieve a better optimization. At each iteration, the geometry gets updated, which requires a meshing step before the FEM simulation can be run. This step adds more computational cost, but it makes the geometry handling fairly straightforward. As long as the geometry generation does not fail after parameter updates, the meshing step is typically unproblematic. It is the designer's duty to ensure that the geometry generation behaves properly for all feasible parameter combinations. The parameter optimization flow chart is shown in Figure 1. A notable

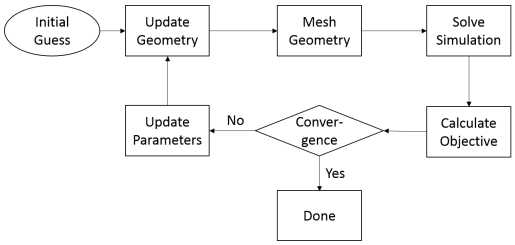

Fig. 1: The flow chart for parameter optimization includes a meshing step at each iteration.

drawback of the re-meshing at each iteration is the fact that the solution of the previous iteration is not directly available. The previous solution is necessary to analytically calculate the sensitivity of the objective function with respect to control parameters, i.e. the gradient of the objective function with respect to control parameters is not explicitly available. Therefore, parameter optimization is typically restricted to gradient-free optimization algorithms to update the parameters. A full review of gradient-based and gradient-free optimization algorithms is not within the scope of this work, but the interested reader can find a thorough discussion in [11]. For the example below, we employed the Nelder-Mead algorithm [12] as it is implemented in the optimization module of the COMSOL Multiphysics software [13].

2.1 Example: Compression Driver Waveguide With Smooth Off-Axis Behavior

High-frequency waveguides are typically used to control the directivity properties of high-frequency components in loudspeakers. For this example, we optimize an in-wall speaker waveguide that is coupled to a high-frequency compression driver of type JBL 2409H. The target is to achieve horizontal and vertical beamwidths of over 100°. Additionally the far-field SPL at off-axis angles should drop monotonically and smoothly.

2.1.1 Geometry Setup & Parameterization

Depth, width and height of the waveguide are fixed at 50 mm, 320 mm, and 170 mm respectively. The throat exit of the compression driver is 14.4 mm in diameter and the waveguide should have symmetry with respect to the horizontal and vertical planes. What remains is to define the waveguide surface in a way that can be described with a set of parameters. For this we

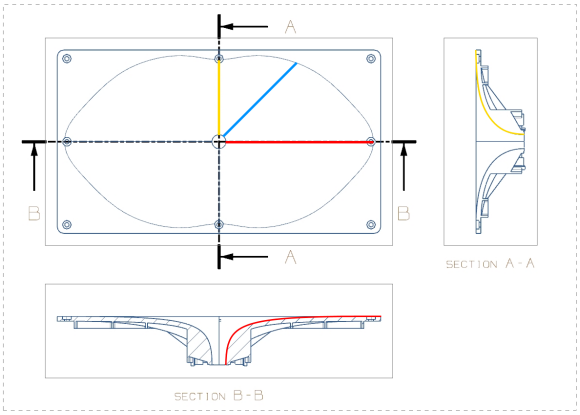

Fig. 2: Horizontal (red), vertical (yellow), and oblique (blue) cross sections that parameterize the waveguide. Throat diameter as well as outer diameter in horizontal and vertical direction are fixed.

define three cross-sectional splines: one in horizontal direction, one in vertical direction and one at the 45° direction (refer to Figure 2). The outer end point in the 45° direction is allowed to vary between a diameter of 170 mm $\leq D^{45}_{mouth} \leq$ 240 mm. Each cross section is described by a cubic Bezier curve defined by four points (see Figure 3). Start point and end point are defined by waveguide depth, throat diameter, and outer diameter. We parameterize the two remaining points by the two parameters L_i and L_o. The two points are chosen such that the throat is tangential to the axial direction and the mouth ends up tangential to the baffle surface.

2.1.2 Objective Function

As stated above, the aim of this waveguide is to have wide beamwidths and smooth off-axis response. For this purpose we define far-field SPL targets relative to on-axis in the 20° and 60° directions, $\hat{\Delta}20(f)$ and $\hat{\Delta}_i60(f)$ that are linear in a log-frequency plot as shown in Figure 4. At 10 kHz, $\hat{\Delta}_{60}$ should be -6 dB and $\hat{\Delta}_{20}$ should be -0.9 dB. The slopes of the target lines in Figure 4 are yet unknown. To deal with these unknowns, it is possible to add additional design parameters and let the optimization algorithm find the best solution. One way to parametrize the target curve is by defining the relative SPL at 1 kHz. The equation for the target lines in Figure 4 thus become:

$$\hat{\Delta}_i(f) = m_i * \log_{10}(f) - C_i \tag{5}$$

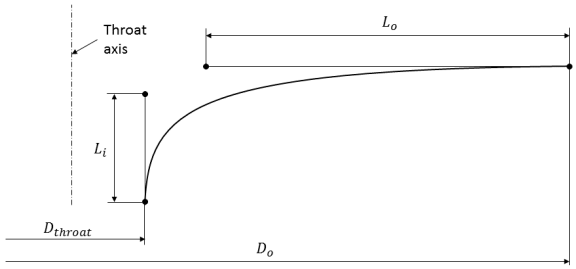

Fig. 3: The cross section curves are parameterized by cubic Bezier curves. The first and last point are given by throat diameter, waveguide depth and outer diameter respectively. The remaining two points are parameterized by the two lengths L_i, and L_o.

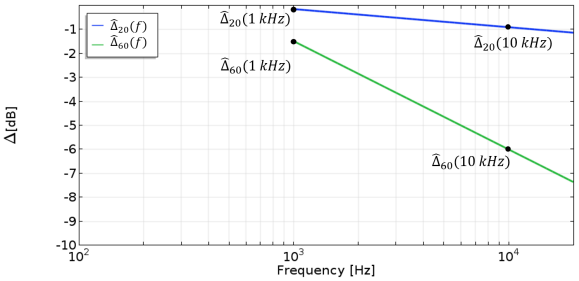

Fig. 4: The off-axis target relative to on-axis at 20° (blue) and 60° (green). At 10 kHz $\hat{\Delta}_{20}$ is -0.9 dB, and $\hat{\Delta}_{60}$ is -6 dB. The values at 1 kHz are taken as additional design parameters.

with

$$m_i = \hat{\Delta}_i(10kHz) - \hat{\Delta}_i(1kHz) \quad (6)$$

$$C_i = \hat{\Delta}_i(10kHz) - 4 * m_i \quad (7)$$

for $i = 20, 60$. Once the design parameters are chosen, we can write the objective function $F(q)$ as the sum of the errors between simulated off-axis responses $\Delta_i(\mathbf{q}, f)$ and target off-axis responses $\hat{\Delta}_i(f)$

$$F(q) = \sum_{m=1}^{M} \Big(\left|\Delta_{20}(\mathbf{q}, f_m) - \hat{\Delta}_{20}(f_m)\right|^p + \left|\Delta_{60}(\mathbf{q}, f_m) - \hat{\Delta}_{60}(f_m)\right|^p \Big) \quad (8)$$

Here, M is the number of frequencies, f_m, that are simulated, and p is an error tuning parameter. If p is equal to 2, then (8) is simply least a squares error between target and simulated off-axis responses. If p is chosen to be a larger number, then frequencies with larger errors are penalized with more weight than frequencies with smaller errors. For this example, we set $p = 4$ to put more emphasis on reducing large peaks in the error between target and simulation.

To finalize the setup, appropriate limits are needed for the design parameters. During the optimization, the design parameters are also normalized to control parameters as shown in (2). The complete list of design parameters is given in Table 1. The simulation ran from 1 kHz to 10 kHz in 11 logarithmically-spaced frequency points.

2.1.3 Simulation Setup

Due to symmetry of the problem, only a quarter of the model needed to be simulated. COMSOL Multiphysics'[13] CAD generating capabilities are not powerful enough to generate the lofted surface needed for this problem, but the LiveLink to SolidWorks allows for a two-way link between SolidWorks [14] and COMSOL. The FEM model was setup to have the mouth of the waveguide terminate into an infinite baffle. At some distance to the waveguide we employed a perfectly matched layer to simulate an infinite 2π environment. The mesh used quadratic elements with at least six elements per wavelength at 10 kHz. The far-field response was calculated using the Kirchhoff-Helmholtz integral at the boundary of the mesh.

2.1.4 Results

The optimization in COMSOL converged to control parameters that correspond to the design parameters shown in Table 1. The horizontal and vertical off-axis plots are shown in Figure 5. From those one can see that we achieved a remarkably smooth and continuous drop of high frequency at all off-axis angles. The simulation achieved a horizontal beamwidth of about 105° and the prototype about 110° (6 dB down at 10 kHz). In the vertical plane, simulation and measurement show a 95° beamwidth. The resulting on-axis response, total soundpower estimate [15, 16, p. 378], and directivity index (DI, shifted by 50 dB) for a plane-wave source with constant amplitude at the throat are shown in Figure 6. This plot also shows a very smooth behavior with a 5-10 dB boost at the high midrange. The DI plot is monotonically and smoothly increasing from 0.8 dB at 1 kHz to 6 dB at 20 kHz.

Parameter	Lower bound	Upper bound	Optimal Solution
L_i^{hor}	5 mm	45 mm	44.37 mm
L_o^{hor}	15 mm	138 mm	137.14 mm
L_i^{vert}	5 mm	45 mm	33.67 mm
L_o^{vert}	8 mm	70 mm	48.52 mm
L_i^{45}	5 mm	45 mm	27.15 mm
L_o^{45}	11 mm	101 mm	38.12 mm
D_o^{45}	168 mm	233 mm	232.6 mm
$\hat{\Delta}_{20}(1kHz)$	-1 dB	-0.01 dB	-0.14 dB
$\hat{\Delta}_{60}(1kHz)$	-2.5 dB	-0.5 dB	-1.48 dB

Table 1: Design parameters for waveguide surface.

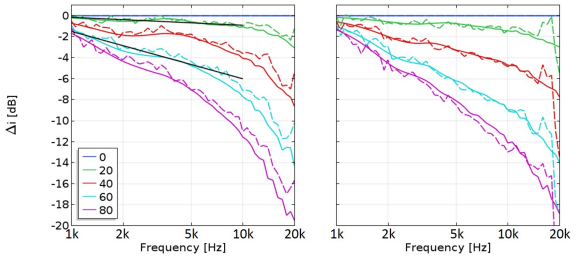

Fig. 5: Horizontal (left) and vertical (right) off-axis results for simulation (solid), measurements of physical prototype (dashed), and target curves for the 20° and 60° angles (black).

2.1.5 Conclusion

Thanks to the parameter optimization of the waveguide, the results of the very first prototype show a remarkably smooth off-axis response. The implementation was made possible thanks to the linked CAD and FEM software and would have been very difficult to achieve otherwise. Setting up this problem as an optimization problem reduced the involvement of the designer dramatically, as only the base geometry and parametrization needed to be defined. Decisions on how deep or shallow to make certain parts of the waveguide were completely handled by the optimization algorithm.

3 Shape Optimization

As mentioned above, one drawback of parameter optimization for geometric design is that it requires a re-meshing step at each iteration and the loss of sensitivity information to control parameters. One optimization method to overcome this drawback is called

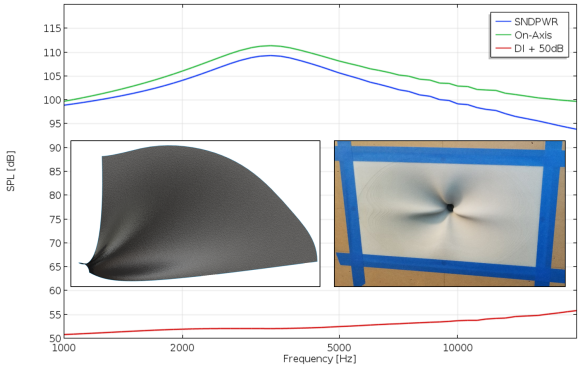

Fig. 6: The on-axis (green), soundpower (blue) and DI (red) response of the waveguide. The units are in dB and the on-axis and soundpower are at arbitrary level. The DI curve is shifted by 50 dB. The insets show the CAD geometry on the left and the prototype mounted in a baffle on the right.

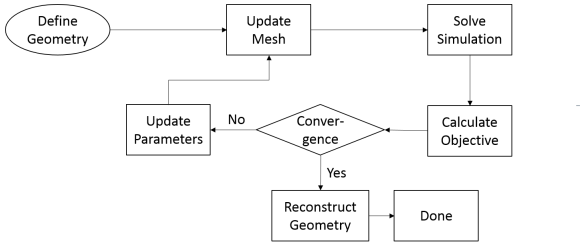

Fig. 7: The flow chart for shape optimization shows how the control parameter update acts directly on the mesh itself. After convergence, there is an additional step needed to obtain the final optimal geometry.

shape optimization (also known as mesh warping, mesh morphing or mesh moving) [17]. During shape optimization, the control parameters act on the mesh nodes instead of on the underlying geometry. This means that the mesh gets warped and squeezed, but throughout all iterations each node retains its relative position with regards to its neighboring nodes. The gradients of the objective function with respect to control parameters can thus be analytically calculated, and we can employ gradient-based optimization schemes [18]. The optimized geometry can finally be reconstructed from the final morphed mesh. The shape optimization flow chart is shown in Figure 7. Typically, mesh deformation is driven at a boundary. The adjacent domain

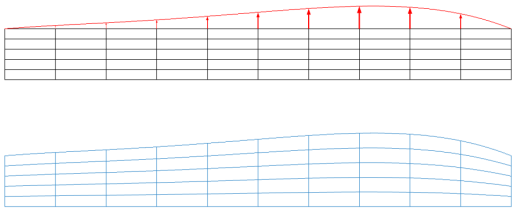

Fig. 8: Original mesh (black) with prescribed deformation at the top boundary (red) and the resulting deformed mesh (blue).

mesh needs to adapt to the prescribed boundary deformation during the mesh update step. There are many algorithms that can be employed for this adaptation, with the more prominent ones being Laplace, Winslow, Yeoh smoothing [19]. Care needs to be taken when the mesh deformations become large, because it can deteriorate the mesh quality or lead to inverted elements.This method works therefore best when small deformations are needed to achieve the optimal solution. Typically, employing rectangular swept meshes leads to more stability and faster convergence [19]. An example of a deformed mesh is shown in Figure 8.

We need to define a parametrization of the boundary displacement with associated control parameters. One suited parametrization is to define the boundary displacements by Bernstein polynomials [20]. Other possible parametrization are Chebyshev polynomials [21] or the Fourier basis just to name a few. The Bernstein basis polynomials of degree n are defined as

$$b_{\nu,n}(x) = \binom{n}{\nu} x^{\nu}(1-x)^{n-\nu}. \tag{9}$$

And the resulting Bernstein polynomial is a linear combination of the individual basis polynomials

$$B_n(x) = \sum_{\nu=0}^{n} \beta_\nu b_{\nu,n}(x) \tag{10}$$

with β_ν the coefficients of the polynomial. These coefficients are excellent candidates for design parameters. Figure 9 shows the Bernstein basis polynomials of degree 4. It also shows that the sum of the five basis polynomials adds up to unity. This is an intrinsic feature of the Bernstein basis polynomials and holds true for any degree n. Additionally we can see that only basis polynomials $b_{0,n}$ and $b_{n,n}$ contribute to the outer points. This is a feature that will be taken advantage of in the next example.

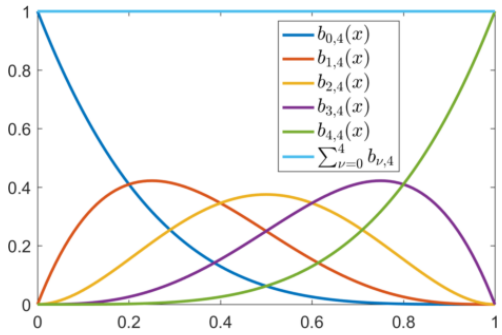

Fig. 9: The Bernstein polynomial basis of degree 4. The sum of the polynomials adds up to unity and only $b_{0,4}$ and $b_{4,4}$ contribute to the edges of the interval (0,1).

3.1 Example: Compression Driver Phase Plug

Compression drivers use a phase plug to reduce the radiating area of a driver's diaphragm to a smaller area of a horn or waveguide throat [22]. The area reduction is typically enforced by putting a phase plug with concentric or radial channels between the diaphragm and the horn throat. Optimal design of the channels reduces resonances in the small air cavity between diaphragm and phase plug. An analytic approach for the optimal selection of concentric channels' location and width has been proposed by Jack Oclee-Brown [23]. However, the method stops short of being directly applicable to channels that meet at a central horn throat, but it does provide an excellent starting point. In the next sections, we show how shape optimization can be used to take an initial solution from [23] and adapt it to a final optimal phase plug geometry.

3.1.1 Geometry Setup & Parametrization

The geometry setup for this example is shown in Figure 10.

The diaphragm is shaped from an elliptical cross section with semi-axes of 35 mm and 27 mm, truncated at a radius of 30 mm. The air cavity in front of the diaphragm is constructed by moving the diaphragm 1 mm in the axial direction, according to [23]. The phase plug terminates into an infinite plane wave tube with radius of $R_{tube} = 10$ mm. The channel location r_i thicknesses t_i at the diaphragm are to be optimized and must

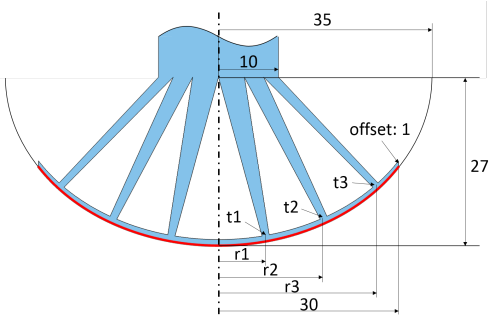

Fig. 10: Geometry setup for compression phase plug. The air (blue) gets compressed from the diaphragm with an truncated elliptical cross section (red) to an infinite tube with radius 10 mm.

adhere to the equation:

$$\sum_{i=1}^{3} 2\pi r_i t_i = \pi R_{tube}^2 \tag{11}$$

The compression ratio is

$$\frac{\int_S n_z dS}{\pi R_{tube}^2} = 9.0 \tag{12}$$

where n_z is the axial component of the diaphragm surface normal, and the integral is taken over the diaphragm surface S. The channel dimensions r_i and t_i can be calculated for straight channels according to [23]. This leads to very close pressure distributions inside each channel as shown in Figure 11. Below 16 kHz, the max difference between the channels is 1.4 dB. In a next step we angled the straight channels to meet at a tube with 10 mm radius as shown in Figure 10. The channel thickness changes towards the tube to maintain the same cross-sectional area $Ai = 2\pi r_i t_i$. After this change in geometry we simulated the pressure inside the plane-wave tube. The simulated tube length is 0.1 m with a perfectly matched layer at the end. The resulting SPL in the tube is also shown in Figure 11.

From Figure 11 it is evident that simply slanting the channels to meet at the throat of a tube is not going to lead to optimal results. This is where shape optimization can help to fine tune the shape of the phase plug. We let the six boundaries highlighted in Figure 12 be morphed by the shape optimization algorithm. Each boundary's deformation is controlled by Bernstein polynomials of degree 4 via the parameters $\beta_\nu^{(s)}$,

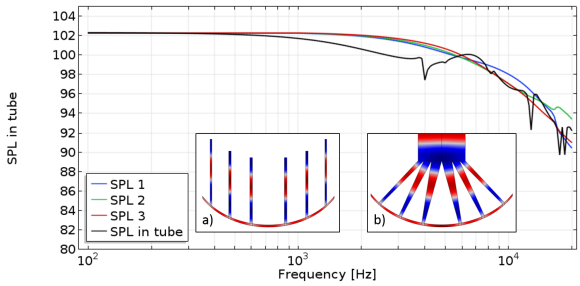

Fig. 11: SPL pressure in the three straight channels optimized according to [23]. The max SPL difference is 1.4 dB at 15.5 kHz. Inset a) shows pressure distribution inside straight channels and inset b) shows the pressure distribution in the slanted channels at 15.5 kHz.

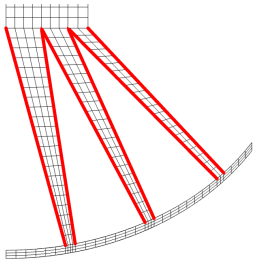

Fig. 12: Mesh and deforming boundaries of the phase plug shown in axisymmetric plot. Each red boundary is mapped onto an interval (0,1) and allowed to deform according to a Bernstein polynomial of degree 4 with β_0 and β_4 fixed at zero.

where (s) denotes the boundary number. By setting $\beta_0^{(s)}$ and $\beta_4^{(s)}$ equal to zero we ensure that the channels endpoints maintain their position throughout the optimization. This leads to 18 remaining parameters

$$\beta_\nu^{(s)}, \nu = \{1,2,3\}, s = \{1,2,\cdots,6\}. \tag{13}$$

3.1.2 Objective Function

The objective is to achieve a smooth frequency response curve in the plane-wave tube. Smoothness is not easily quantified with mathematical formulas, but a good alternative would be to try to achieve a frequency response curve that is the average of the three frequency

response curves achieved with the straight channels as shown in Figure 11.

$$SPL_{target}(f) = \frac{SPL_1(f) + SPL_2(f) + SPL_3(f)}{3} \quad (14)$$

We implemented this target as a least-squares problem over M number of frequencies f_m.

$$F(\mathbf{q}) = \sum_{m=1}^{M} \left(SPL_{tube}(\mathbf{q}, f_m) - SPL_{target}(f_m) \right)^2 \quad (15)$$

3.1.3 Simulation Setup

In order to reduce the chance for the channels to collapse or overlap, we restricted the design parameters to the interval $\beta_v^{(s)} \in (-0.004, 0.004)$. The design parameters $\beta_v^{(s)}$ are themselves mapped to control parameters according to (2). In COMSOL the deforming mesh can be set up fairly easily once a parametrization is chosen and linear mappings between the morphing boundaries and the interval (0,1) is established. We used the default mesh update settings (Yeoh) and ran the optimization with the gradient-based SNOPT [24] solver.

3.1.4 Results

The optimizer quickly converged towards a solution that exhibits a very smooth frequency response in the plane-wave tube. The SPL curve and pressure plot are shown in Figure 13. The inset also shows the deformed mesh of the channels. The maximal deviation from the target curve is 0.8 dB, which confirms the choice of the average straight-channel pressures as a viable target. The deformed mesh shows that channels 2 and 3 get very close to each other towards the tube. An overlap of the meshes is not ruled out by the choice of parameter limits. It is up to the designer to check for mesh overlap or collapse before continuing with the optimized geometry.

3.1.5 Conclusion

Shape optimization problems require more time and effort to set up than parameter optimization problems. The advantage is that they generally converge faster towards an optimal solution because they can profit from the analytic gradient calculation, which is not possible in parameter optimization. The obtained optimal mesh

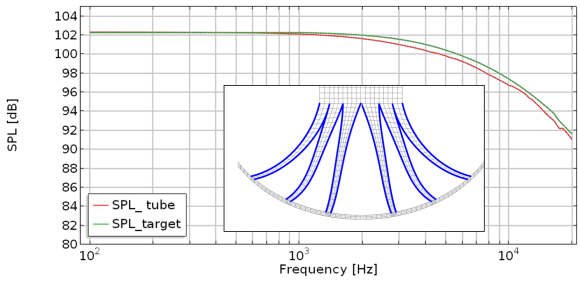

Fig. 13: SPL and SPL target in the plane wave tube after optimization. A very smooth frequency response is obtained and the maximum difference between obtained SPL and target is 0.8 dB. The inset shows the deformed mesh at the end of the optimization with the deformed boundaries shown in blue.

needs to be checked for overlap and translated into a finalized geometry. We show that mesh optimization can improve upon the already excellent analytic prediction for straight tubes towards a more realistic phase plug geometry that attaches to a plane-wave tube or horn. It remains to be seen if higher-degree polynomials or a different basis could lead to even better results.

4 Topology Optimization

Shape optimization and parameter optimization require to some extent that the topology (i.e., arrangement of holes, intersections etc.) be defined a priori and maintained during the optimization. When the optimal topology is not yet known, topology optimization can be employed to find an optimal geometry [25]. Topology optimization originated in structural mechanics where it was developed to find the optimal material distribution while maintaining a given compliance of a structure under given load. It has since also been adapted for acoustic problems [26, 27, 28]. The idea is to optimally place a given amount of material inside a design subdomain. Each point in the subdomain can take on a material property that is interpolated between two materials, typically a solid and air or void. With the discretization of the domain with finite elements, the interpolation variable takes on the form of a vector with an entry for each node in the mesh. The general strategy for acoustic problems is the following:
1) Define a subdomain Ω_d of the simulation domain where you want to distribute solid and air. 2) Determine

a relevant material property that can be interpolated between the values of the two different materials, e.g., density ρ and bulk modulus K with subscript 0 for air and subscript 1 for some solid:

$$\rho(\mathbf{q}) = \begin{cases} \rho_0 \text{ for } q_i = 0 \text{ (air)} \\ \rho_1 \text{ for } q_i = 1 \text{ (solid)} \end{cases} \tag{16}$$

$$K(\mathbf{q}) = \begin{cases} K_0 \text{ for } q_i = 0 \text{ (air)} \\ K_1 \text{ for } q_i = 1 \text{ (solid)} \end{cases} \tag{17}$$

3) Determine a suitable material interpolation scheme that defines the interpolated material properties for values of $\mathbf{q}$ between 0 and 1. The easiest interpolation would be a linear interpolation, but that is not always the optimal choice. Better choices are discussed below.
4) Define a domain constraint that limits the total amount of solid material that can be placed inside the subdomain to a relative number δ with the inequality constraint

$$\frac{\int_{\Omega_d} \mathbf{q} d\tilde{\Omega}}{\int_{\Omega_d} d\tilde{\Omega}} \leq \delta \tag{18}$$

e.g., if δ is chosen to be 0.5, then half of the domain can be filled with solid material.
5) Define an objective function and optimization algorithm.
6) Interpret the material distribution and define a final geometry.

4.1 Example: Tweeter Phase Plug for High-Frequency Extension

Transducer engineers at the Samsung Audio Lab have designed a tweeter that can play as low as 500 Hz, and it is likely to be put into several commercial products. Its main advantage is a low frequency cross-over that minimizes lobing and thus creates a wider sweet spot for the listeners. The problem with this tweeter is that the frequency response drops significantly around 18 kHz. We could replicate this behavior with coupled acoustic-structural FEM simulations after careful selection of material parameters. Measured and simulated frequency response curves are shown in Figure 14. An investigation into the root cause of the drop at 18 kHz revealed a structural resonance in the surround that destructively coupled with the pressure generated by the diaphragm that moves pistonically up to 23 kHz. A snapshot of the surround deformation (exaggerated)

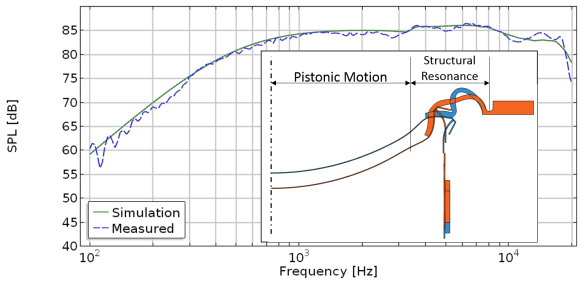

Fig. 14: Simulated (green) and measured (blue) frequency response of tweeter show an very good match, including drop-off at 18 kHz. The inset shows simulated surround deformation at 20 kHz at 0° (blue) and 180° (orange). The deformation is exaggerated by a factor of 2000. The diaphragm moves pistonically and the surround exhibits a resonance.

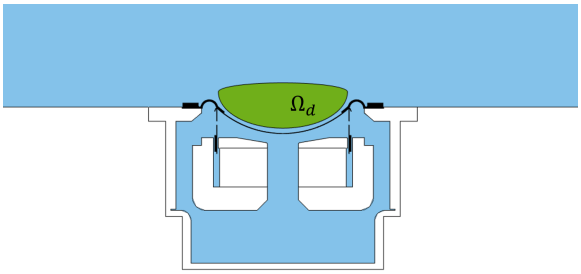

Fig. 15: Design subdomain Ω_d (green), air (blue) and tweeter geometry (black).

at 20kHz is shown in the inset of Figure 14. A solution to the described problem could be to re-design the surround. But we wanted to investigate acoustic solutions, since the performance of the driver below 18 kHz is excellent and first attempts to fix the problem at the surround deteriorated the performance at lower frequencies.

4.1.1 Geometry Setup and Parametrization

Topology optimization does not require the parametric design of the geometry or mesh deformation. We only need to define the subdomain Ω_d, where the algorithm needs to optimize the material distribution. The Ω_d for the tweeter at hand is shown in Figure 15. The air domain was surround by perfectly matched layers to avoid reflections . The parametrization for the optimization is done in the material interpolation. As mentioned

above, we need to define an interpolation of the material properties inside Ω_d. The two most widely used interpolation functions are the so-called SIMP [29] and RAMP [30] interpolation methods. For the example at hand, we used the a slightly modified version of RAMP as presented in [26] for the interpolation of material in Ω_d.

$$\rho(\mathbf{q}) = \frac{\rho_0}{1+\mathbf{q}(\rho_0/\rho_1 - 1)} \tag{19}$$

$$K(\mathbf{q}) = \frac{k_0}{1+\mathbf{q}(K_0/K_1 - 1)} \tag{20}$$

with ρ_0 = 1.204 kg/m^3, K_0= 0.1461 MPa, ρ_1 = 1200 kg/m^3, K_1 = 10 GPa. The choice of the modified interpolation scheme in [26] is based on empirical tests, and we found it to work the best.

4.1.2 Objective Function

The target is to keep the SPL in the listening window [16, p. 378] $SPL_{LW}(f)$ of the tweeter at 85 dB up to 20 kHz. Additionally, we also need to keep the directivity index $DI(f)$ in check, as not to create some highly focused beam at higher frequency. We thus have two objective functions in the form of least squares

$$F(\mathbf{q}) = F_1(\mathbf{q}) + F_2(\mathbf{q}) \tag{21}$$

$$F_1(\mathbf{q}) = \sum_{m=1}^{M} \left(SPL_{LW}(\mathbf{q}, f_m) - 85\right)^2 \tag{22}$$

$$F_2(\mathbf{q}) = \sum_{m=1}^{M} \left(DI(\mathbf{q}, f_m) - \hat{DI}(f_m)\right)^2 \tag{23}$$

where $\hat{DI}(f)$ is a target for the directivity index as shown in Figure 17 and M is the number of frequency points f_m to include in the simulation.

4.1.3 Simulation Setup

After defining the design subdomain Ω_d, the material interpolation functions and the objective function, we define the initial value of the parameter field $\mathbf{q}$ at 0.5 and choose δ from (18) to be 1, i.e., potentially all of Ω_d could be filled with solid material. The solver method of choice for topology optimization is the Method of Moving Asymptotes (MMA)[31], because it handles a large number of control variables well. Remember, the value of $\mathbf{q}$ at each mesh node in Ω_d, is now a control variable. The optimization was performed over 6th-octave points between 5 kHz and 20 kHz. The final results were then recomputed over 24th-octave points between 100 Hz and 20 kHz.

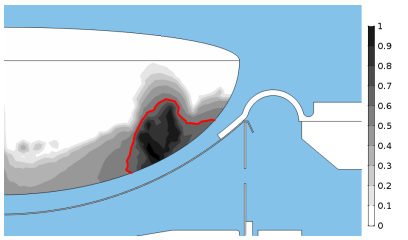

Fig. 16: Final distribution of control parameter $\mathbf{q}$ in shaded grey. The shades of grey change in increments of 0.1 from 0 to 1. The contour of level $\mathbf{q}_c$ = 0.6 is shown in red.

4.1.4 Results

The resulting distribution of $\mathbf{q}$ is shown in Figure 16. The topology optimization results in a distribution of $\mathbf{q}$ that varies between 0 (white) and 1 (black). After the topology optimization provided that result, we ran a parameter sweep with a cutoff value of $\mathbf{q}_c$ and set the material values to either air or solid according to

$$\rho(\mathbf{q}) = \begin{cases} \rho_0 \text{ if } \mathbf{q} < \mathbf{q}_c \\ \rho_1 \text{ if } \mathbf{q} \geq \mathbf{q}_c \end{cases} \tag{24}$$

and accordingly for $K(\mathbf{q})$. We found that a value of $\mathbf{q}_c$ = 0.6 (see Figure 16) gives the best compromise for both of the objective functions. From Figure 17 we can see that the topology optimization raised the SPL between 7 kHz and 20 kHz to above 85 dB throughout (solid green), while maintaining an error less than 2 dB for the DI. The interpretation with $\mathbf{q}$ = 0.6 (dashed green) exhibits a drop in SPL between 8 kHz and 15 kHz, but it never drops to a value that is lower than the tweeter without the phase plug (orange). The main target of boosting the SPL above 18 kHz has been achieved and DI curve is practically identical for both cases.

4.1.5 Conclusion

Topology optimization is not yet common practice in loudspeaker design, but it can be helpful when the optimal topology is not easily guessed a priori. It also requires some experimentation with interpolation functions and constraint settings to get acceptable results. We have shown that it can be used for the design of phase plugs and the method can be easily adapted for other problems. While the results of the material distribution must be interpreted, they can provide a good starting point for a subsequent parameter or shape optimization.

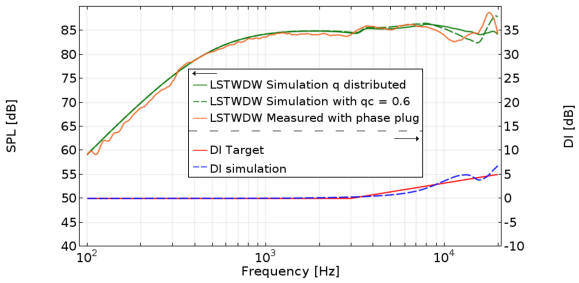

Fig. 17: Results of topology optimization. Solid lines show results with distributed $\mathbf{q}$ after topology optimizaton and dashed lines show results after simulation with cutoff $\mathbf{q}_c = 0.6$. The response of the measured tweeter with the prototype phase plug is shown in orange. The target DI curve is shown in red.

5 Summary

The work presented introduces the three optimization methods and confirmed their viability for the design of acoustic elements in loudspeakers. Parameter optimization is the easiest to implement, because it just requires parameterizing the geometry. It comes with the drawback that the gradient of the objective function cannot be calculated analytically. We implemented a parameter optimization for the optimization with optimal off-axis behavior, and verified the results with the measurement of a prototype. Shape optimization requires slightly more preparation work as the design parameters act on the mesh and care must be taken that the deformation does not lead to invalid geometries. We have implemented a shape optimization example for the design of an optimal compression-driver phase plug that is coupled to a plane-wave tube. Topology optimization is the least intuitive of the three methods and requires the most user input. It can potentially lead to geometries that a designer would not easily conceive otherwise. We have demonstrated the method with the example of a tweeter phase plug that extended the extended the HF range of the tweeter past 20 kHz.

6 Acknowledgements

Samsung Electronics and Samsung Research America supported this work. The author would like to thank the entire staff of Samsung's US Audio Lab who helped with the measurement setup, offered insightful suggestions, reviewed the manuscript and contributed to this work.

References

[1] Dodd, M., "Optimum Diaphragm and Waveguide Geometry for Coincident source Drive Units," in *Audio Eng. Soc. Conv. 121*, 2006.

[2] Murphy, D. and Morgans, R., "Modelling Acoustic Horns with FEA," *Audio Eng. Soc. Conv. 128*, 2010.

[3] Devantier, A. and Rapoport, Z., "Analysis and Modeling of the Bi-Directional Fluid Flow in Loudspeaker Ports," in *Audio Eng. Soc. Conv. 117*, 2004.

[4] Kaizer, A. J. M. and Leeuwestein, A., "Calculation of the Sound Radiation of a Nonrigid Loudspeaker Diaphragm Using the Finite-Element Method," *J. Audio Eng. Soc.*, 36(7/8), pp. 539–551, 1988.

[5] Bezzola, A. and Brunet, P., "Fully coupled time-domain simulations of loudspeaker transducer motors," in *141st Audio Eng. Soc. Int. Conv. 2016, AES 2016*, p. 9599, Los Angeles, 2016.

[6] Bezzola, A., Brunet, P., and Shenli, Y., "Variable Fractional Order Analysis of Loudspeaker Transducers: Theory, Simulations, Measurements, and Synthesis," in *143rd Audio Eng. Soc. Int. Conv. 2017, AES 2017*, p. 9839, New York City, 2017.

[7] Voishvillo, A. and Mazin, V., "Finite-Element Method of Modeling of Eddy Currents and Their Influence on Nonlinear Distortion in Electrodynamic Loudspeakers," in *Audio Eng. Soc. Conv. 99*, 1995.

[8] Dodd, M., "The Development of a Forward Radiating Compression Driver by the Application of Acoustic, Magnetic and Thermal Finite Element Methods," in *Audio Eng. Soc. Conv. 115*, 2003.

[9] Salvatti, A., "Virtual Acoustic Prototyping—Practical Applications for Loudspeaker Development," in *Audio Eng. Soc. Conv. 129*, p. 8213, 2010.

[10] Gill, P. E., Murray, W., and Wright, M. H., *Practical Optimization*, Academic Press, 1981, ISBN 0-12-283952-8.

[11] Nocedal, J. and Wright, S. J., *Numerical Optimization*, Springer Verlag, New York, 2nd edition, 2006, ISBN 0-387-30303-0.

[12] Conn, A. R., Scheinberg, K., and Vicente, L. N., *Introduction to Derivative-Free Optimization*, SIAM, 2009, ISBN 978-0-898716-68-9.

[13] "COMSOL Multiphysics v. 5.3a," 2017.

[14] "SolidWorks 2017," 2017.

[15] Celestinos, A., Devantier, A., Bezzola, A., Banka, R., and Brunet, P., "Estimating the total sound power of loudspeakers," in *139th Audio Eng. Soc. Int. Conv. AES 2015*, p. 9463, New York City, 2015.

[16] Toole, F. E., *Sound Reproduction*, Focal Press, Burlington, MA, 3 edition, 2013, ISBN 978-0-240-52009-4.

[17] Staten, M. L., Owen, S. J., Shontz, S. M., Salinger, A. G., and Coffey, T. S., "A Comparison of Mesh Morphing Methods for 3D Shape Optimization," in *Proc. 20th Int. Meshing Roundtable*, January, pp. 293–311, Springer, Berlin, Heidelberg, 2011, doi:10.1007/978-3-642-24734-7_16.

[18] Frey, W., *Designing New Structures With Shape Optimization*, https://www.comsol.com/blogs/designing-new-structures-with-shape-optimization/, 2015.

[19] COMSOL, "Deformed Geometry and Moving Mesh," in *COMSOL Multiphysics Ref. Man. v. 5.3a*, p. 985, www.comsol.com, 2017.

[20] Wikipedia.org, *Bernstein polynomial*, https://en.wikipedia.org/wiki/Bernstein_polynomial, July 17, 2018.

[21] Wikipedia.org, *Chebyshev polynomial*, https://en.wikipedia.org/wiki/Chebyshev_polynomials, July 17, 2018.

[22] Hanna, C. and Slepian, J., "The Function and Design of Horns for Loudspeakers (Reprint)," *J. Audio Eng. Soc*, 25(9), pp. 573–585, 1977.

[23] Oclee-Brown, J., "A General Approach for the Acoustic Design of Compression Drivers with "Narrow" Channels and Rigid Diaphragms," in *Audio Eng. Soc. Conv. 137*, 2014.

[24] Gill, P. E., Murray, W., and Saunders, M. A., "SNOPT: An SQP algorithm for large-scale constrained optimization," *SIAM Rev.*, 47, pp. 99—-131, 2005.

[25] Bendsøe, M. P. and Sigmund, O., *Topology Optimization*, Springer Verlag Berlin Heidelberg, Berlin, Heidelberg, 2004, ISBN 978-3-642-07698-5, doi:10.1007/978-3-662-05086-6.

[26] Dühring, M. B., Jensen, J. S., and Sigmund, O., "Acoustic design by topology optimization," *J. Sound Vib.*, 317(3-5), pp. 557–575, 2008, ISSN 0022460X, doi:10.1016/j.jsv.2008.03.042.

[27] Christensen, R., *How to Use Acoustic Topology Optimization in Your Simulation Studies*, https://www.comsol.com/blogs/how-to-use-acoustic-topology-optimization-in-your-simulation-studies/, 2016.

[28] Christensen, R., *Acoustic Topology Optimization with Thermoviscous Losses*, https://www.comsol.com/blogs/acoustic-topology-optimization-with-thermoviscous-losses/, 2018.

[29] Bendsøe, M. P., "Optimal shape design as a material distribution problem," *Struct. Optim.*, 1(4), pp. 193–202, 1989, ISSN 09344373, doi:10.1007/BF01650949.

[30] Stolpe, M. and Svanberg, K., "An alternative interpolation scheme for minimum compliance topology optimization," *Struct. Multidiscip. Optim.*, 22(2), pp. 116–124, 2001, ISSN 1615-147X, doi:10.1007/s001580100129.

[31] Svanberg, K., *MMA and GCMMA – Fortran versions March 2013*, KTH, Royal Institute of Technology, Stockholm, 2013.